Optimally Coherent Kerr Combs Generated with Crystalline Whispering Gallery Mode Resonators for Ultrahigh Capacity Fiber Communications

Joerg Pfeifle,[1,2] Aurélien Coillet,[3,*] Rémi Henriet,[3] Khaldoun Saleh,[3] Philipp Schindler,[1] Claudius Weimann,[1] Wolfgang Freude,[1,2] Irina V. Balakireva,[3] Laurent Larger,[3] Christian Koos,[1,2,†] and Yanne K. Chembo[3,‡]

[1]*Institute of Photonics and Quantum Electronics (IPQ), Karlsruhe Institute of Technology (KIT), 76131 Karlsruhe, Germany*

[2]*Institute of Microstructure Technology (IMT), Karlsruhe Institute of Technology (KIT), 76131 Karlsruhe, Germany*

[3]*FEMTO-ST Institute (CNRS UMR6174), Optics Department, 15B Avenue des Montboucons, 25030 Besançon cedex, France*

(Received 5 August 2014; published 2 March 2015)

Optical Kerr frequency combs are known to be effective coherent multiwavelength sources for ultrahigh capacity fiber communications. These combs are the frequency-domain counterparts of a wide variety of spatiotemporal dissipative structures, such as cavity solitons, chaos, or Turing patterns (rolls). In this Letter, we demonstrate that Turing patterns, which correspond to the so-called primary combs in the spectral domain, are optimally coherent in the sense that for the same pump power they provide the most robust carriers for coherent data transmission in fiber communications using advanced modulation formats. Our model is based on a stochastic Lugiato-Lefever equation which accounts for laser pump frequency jitter and amplified spontaneous emission noise induced by the erbium-doped fiber amplifier. Using crystalline whispering-gallery-mode resonators with quality factor $Q \sim 10^9$ for the comb generation, we show that when the noise is accounted for, the coherence of a primary comb is significantly higher than the coherence of their solitonic or chaotic counterparts for the same pump power. In order to confirm this theoretical finding, we perform an optical fiber transmission experiment using advanced modulation formats, and we show that the coherence of the primary comb is high enough to enable data transmission of up to 144 Gbit/s per comb line, the highest value achieved with a Kerr comb so far. This performance evidences that compact crystalline photonic systems have the potential to play a key role in a new generation of coherent fiber communication networks, alongside fully integrated systems.

DOI: 10.1103/PhysRevLett.114.093902 PACS numbers: 42.65.Hw, 42.65.Ky, 42.81.Uv, 84.40.Ua

There is currently vigorous interest in advanced modulation formats for optical fiber communications, powered by the perspective of an ever-growing bandwidth demand. Ultradense optical fiber networks aim to satisfy this demand by using wavelength and polarization multiplexing on highly coherent, evenly spaced carriers. However, it becomes increasingly difficult and costly to generate several such independent but frequency-locked subcarriers when they have to be controlled precisely and individually.

An elegant solution to circumvent this drawback is to use a Kerr optical frequency comb [1]. It is obtained by pumping a whispering-gallery-mode (WGM) resonator with a continuous-wave laser. Above a certain threshold, the strong modal confinement in the torus-shaped eigenmodes and the long photon lifetime enhance the Kerr nonlinear interaction, thereby exciting several WGMs through a hyperparametric interaction [2–4]. Indeed, these combs have proven to be a versatile multiwavelength coherent source for a wide range of applications, and they have been in the focus of a large number of theoretical and experimental works recently [1–10].

In the context of optical communications, Kerr combs have already delivered milestone performances. For example, the early experiments presented in Refs. [11,12] featured single-channel 10 Gbit/s transmissions using an on-off keying modulation scheme. In a more recent publication, the exceptional performance of 1.44 Tbit/s was demonstrated using quadrature phase shift keying and multiplexing 20 channels operating at a bit rate of 72 Gbit/s [13]. In all cases, the combs were generated using integrated (chip scale) silicon nitride resonators with loaded Q-factor of the order of 10^6 at the pumping wavelength of 1550 nm.

Earlier work on Kerr combs has shown that, depending on the pumping conditions (laser frequency and power), various regimes with respect to the dynamics of the system can be theoretically and experimentally observed [14–16]. One of the most interesting dynamical states is the regime of Turing patterns [17] which corresponds to an integer number of rolls (intensity extrema) oscillating along the azimuthal direction of the disk. In the spectral domain, these patterns yield an optical frequency comb with multiple free-spectral range (FSR) spacing, which is sometimes referred to as a *primary comb* in the literature. Beside Turing patterns, other dynamical regimes can be observed as well in the time domain (solitons, chaos, and breathers, for example), leading in the spectral domain to Kerr combs with very different coherence and robustness properties.

The suitability of these various types of Kerr combs for the purpose of optical communications is still to be

investigated in more detail. In this Letter, we show that optical Turing patterns provide frequency combs that are optimally suited for high-speed data transmission using advanced modulation formats. In particular, we compare the coherence properties of a Turing pattern with a soliton and a chaotic Kerr comb. Our results show that Turing patterns are more robust against frequency and amplitude noise of the pump laser and exhibit the highest coherence between the individual comb lines. We experimentally verify the robustness and low-noise levels of the Turing pattern in a data transmission experiment. We achieve a per-channel data rate of 144 Gbit/s. In comparison to Ref. [13], these experiments did not require a feedback loop to maintain the comb state, which underlines the robustness of the Turing pattern. In addition, the high quality of the WGM resonator allows for a significant reduction of the pump power.

For Kerr comb generation, we consider a millimeter-sized ultrahigh Q crystalline WGM resonator pumped around 1550 nm. The loaded quality factor of this magnesium fluoride (MgF_2) resonator is typically higher than 10^9. The fundamental eigenmodes of the WGM resonators are quasiequidistant and separated by the free-spectral range $\Omega_{\mathrm{FSR}}/2\pi = c/(n_g \pi d)$, where c is the velocity of light in vacuum, d is the diameter of the disk, and n_g is its frequency-dependent group velocity refractive index at the pump wavelength.

The total intracavity field is the sum of all these modal contributions, and its spatiotemporal dynamics can be modeled using the Lugiato-Lefever equation (LLE) [18],

$$\frac{\partial \psi}{\partial \tau} = -(1 + i\alpha)\psi + i|\psi|^2\psi - i\frac{\beta}{2}\frac{\partial^2 \psi}{\partial \theta^2} + F, \qquad (1)$$

where $\psi(\theta, \tau)$ is the normalized complex slowly varying envelope of the intracavity field, with $|\psi|^2$ being proportional to the number of intracavity photons [19–21]. The dimensionless time τ is normalized to $2\tau_{\mathrm{ph}} = 2Q_{\mathrm{tot}}/\omega_L$, where τ_{ph} is the photon lifetime, ω_L is the angular frequency of the pump laser, $Q_{\mathrm{tot}} = [Q_{\mathrm{in}}^{-1} + Q_{\mathrm{ext}}^{-1}]^{-1} \simeq 1.3 \times 10^9$ is the loaded (total) quality factor, and $Q_{\mathrm{in,ext}}$ are the intrinsic and extrinsic quality factors. The angular variable θ is the azimuthal coordinate along the circumference of the disk resonator. The parameter α stands for the frequency detuning between the laser and the cold-cavity resonance, while β represents the normalized second-order (group velocity) dispersion. The square of the dimensionless pump term F in Eq. (1) is proportional to the laser power P. Laser pump frequency jitter and amplified spontaneous emission noise (induced by the optical amplifier) can be accounted for by replacing α by $\alpha + \xi_m(\tau)$, and F by $F + \zeta_a(\theta, \tau)$, respectively. The Gaussian white noise terms $\xi_m(\tau)$ (frequency noise) and $\zeta_a(\theta, \tau)$ (amplified spontaneous emission noise), which are real- and complex-valued, respectively, have autocorrelations

$$\langle \xi_m(\tau)\xi_m(\tau')\rangle = 2D_m\delta(\tau - \tau') \qquad (2)$$

$$\langle \zeta_a(\theta, \tau)\zeta_a^*(\theta', \tau')\rangle = 4D_a\delta(\theta - \theta')\delta(\tau - \tau'), \qquad (3)$$

with δ being the Dirac function, while $D_{a,m}$ is a measure of the spectral power density of the noise. Note that we have assumed uncorrelated spatial and temporal noises in $\zeta_a(\theta, \tau)$, which can include a very large variety of physical noises [22,23].

It has already been proven that no Kerr comb can be generated when the pump power is such that $F^2 < 1$ [15]. In the anomalous dispersion regime ($\beta < 0$), the LLE analysis shows that when the laser pumping power is increased, the Turing patterns arise through a bifurcation which in the context of bifurcation analysis is referred to as a $(i\omega)^2$, a Hamiltonian-Hopf, or a Turing bifurcation [15]. The corresponding critical pump power is then $F^2 = 1 + (\alpha - 1)^2$ for $\alpha < 2$, and the number of Turing rolls at threshold is analytically determined as the closest integer approximation of $l_{\mathrm{th}} = [(2/\beta)(\alpha - 2)]^{1/2}$. In the spectral domain, the corresponding comb features equidistant lines with intermodal frequency $l_{\mathrm{th}} \times \Omega_{\mathrm{FSR}}$. On the other hand, for $\alpha > \sqrt{3}$, increasing the pump power leads to the subcritical excitation of solitons as soon as $F^2 \simeq \alpha$. In both cases, when the laser pump power is sufficiently high, the Kerr comb always becomes chaotic [14,15,24,25].

When optical noise is accounted for, our stochastic LLE is numerically simulated using a combination of the Euler-Maruyama and the adaptive split-step Fourier algorithms. A number N of cavity snapshots $\{\psi_1, \ldots, \psi_N\}$ is periodically recorded at times $\tau_m = mT_{\mathrm{rec}}$ ($T_{\mathrm{rec}} \sim 1$), so that $\psi_m(\theta) \equiv \psi(\theta, \tau_m)$. Once the transients have been skipped, the coherence of the spatiotemporal dynamics can be defined in the asymptotic limit $N \gg 1$ as

$$\chi = \frac{1}{N}\sum_{k=0}^{N-1} |\hat{g}_k^{(1)}|^2, \qquad (4)$$

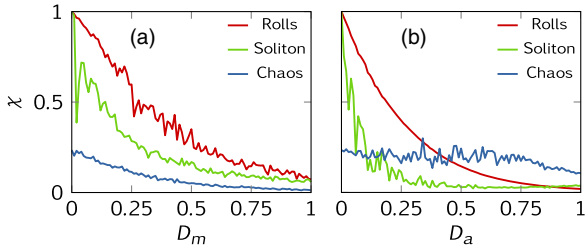

FIG. 1 (color online). Variation of the coherence as a function of (a) frequency noise and (b) amplified spontaneous emission noise. In both cases, the normalized pump power according to Eq. (1) was kept constant at $F^2 = 11$, and the normalized second-order (group velocity) dispersion was fixed at $\beta = -0.04$. The frequency detuning α is equal to -1.5 (Turing rolls), 2 (chaos), and 9 (soliton). Note that chaos is always partially incoherent, even in the absence of optical noise.

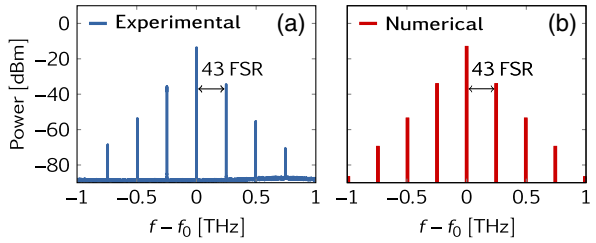

FIG. 2 (color online). Experimental and simulated spectra of the ultrastable Turing pattern used for the experiment. The resonator was a magnesium fluoride (MgF_2) disk with intrinsic quality factor $Q_{in} = 1.5 \times 10^9$ and group refractive index $n_g = 1.37$ at the pump wavelength $\lambda_L = 2\pi c/\omega_L = 1552.0$ nm. Its diameter was $d = 11.3$ mm, yielding a free-spectral range $\Omega_{FSR}/2\pi = 5.78$ GHz. In the figure, the Turing pattern of 43rd order has been excited, and the spectral distance between excited modes is therefore 248.54 GHz. The order of the Turing pattern can be tuned through the pump power or frequency [15]. The pump power was 295 mW, measured at the input of the tapered fiber which is coupled to the resonator with an extrinsic quality factor $Q_{ext} = 8.5 \times 10^9$. (a) Experimental spectrum. (b) Corresponding numerical simulation of Eq. (1), with $\alpha = -1$, $\beta = -4.3 \times 10^{-3}$, and $F^2 = 11$. An excellent agreement between theoretical and experimental spectra is achieved.

where

$$\hat{g}_k^{(1)} = \frac{\frac{1}{N-k}\sum_{m=k+1}^{N}\int_{-\pi}^{+\pi}\psi_m(\theta)\psi_{m-k}^*(\theta)d\theta}{\frac{1}{N}\sum_{m=1}^{N}\int_{-\pi}^{+\pi}\psi_m(\theta)\psi_m^*(\theta)d\theta} \qquad (5)$$

is the discrete first-order coherence function [26].

The real-valued coherence parameter χ is equal to 1 for a perfectly periodic signal, and steadily decreases to 0 as the signal becomes increasingly incoherent. The variation of χ as a function of optical noise power is displayed in Fig. 1. It appears clearly that for realistic (i.e., low) noise conditions, coherence is always higher for Turing patterns than for solitons and chaos. Interestingly, as the noise is increased, the coherence parameter χ decreases slower for rolls than it does for solitons. This proves that rolls are particularly robust to noise perturbations and remain highly coherent (strongly phase-locked) even when mixed with high levels of optical noise. Noise in experimental conditions is sufficiently low ($D_{a,m} < 0.1$) for the Turing patterns to be significantly more coherent than its chaotic or solitonic counterparts.

In order to confirm this theoretical finding, we have performed a transmission experiment with primary combs originating from ultrahigh Q crystalline WGM resonators. The power spectrum used for our coherent transmission experiments is presented in Fig. 2. As emphasized earlier, these combs are very robust and strongly phase-locked [25]. In particular, their spectral purity is exceptionally high, and typically very close to that of the pumping laser. They can therefore be used as carriers in an ultrahigh capacity wavelength division multiplexing (WDM) network, as described below.

The full experimental setup is displayed in Fig. 3. We use only three modes of the comb, namely the center mode (labeled as line 0) and its two immediately adjacent side modes (lines −1 and +1). We use quadrature phase shift keying (QPSK) or 16-state quadrature amplitude

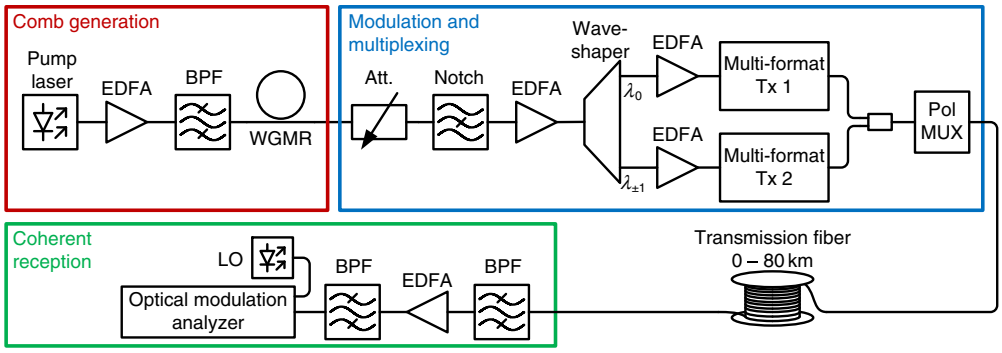

FIG. 3 (color online). Schematic representation of the experimental setup for data transmission. The Turing pattern generator comprises a tunable laser, an erbium-doped fiber amplifier (EDFA) and a bandpass filter (BPF) that rejects amplified spontaneous emission noise from the EDFA. A notch filter attenuates the center mode to a level comparable to the first-order side modes of the comb. A programmable filter is used for interleaving, flattening, and filtering the comb lines. Two EDFAs boost the carriers, which are fed via polarization controllers (PC) to two multiformat transmitters (Tx × 1 for comb line 0, and Tx 2 for comb lines ±1). After encoding of uncorrelated data onto the carriers at a symbol rate of 18 GBd, the two data streams are merged. To emulate polarization multiplexing (PolMUX), we create two time-delayed copies of the pseudorandom data stream and superimpose them on two orthogonal polarization states of the standard single-mode transmission fiber. We insert different lengths of transmission fiber, ranging from a few meters to 80 km. At the receiver, the data stream passes through bandpass filters and an EDFA before being coherently detected with an external cavity laser serving as a local oscillator (LO). The LO is tuned to match the center frequency of the respective channel and an optical modulation analyzer is used to monitor the quality of the received signal. The received data are visualized using constellation diagrams that display the real and the imaginary part of the optical amplitude in the complex plane.

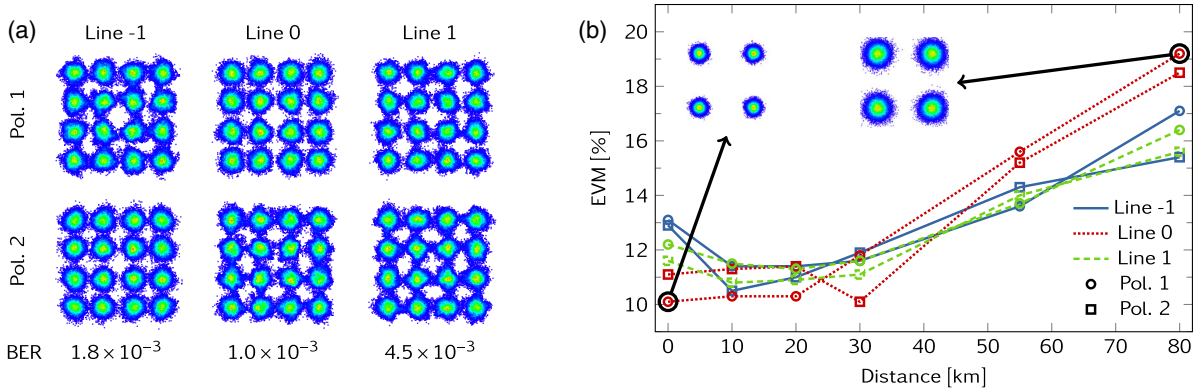

FIG. 4 (color online). Results of the data transmission experiments. (a) Back-to-back experiment at 144 Gbit/s per wavelength channel using 16QAM. The 16 constellation points are clearly distinguishable for each comb line and each polarization, indicating sufficiently low error-vector magnitude (EVM) and bit-error ratio (BER). After using forward-error correction (FEC) codes, a BER smaller than 4.5×10^{-3} guarantees error-free transmission (BER $< 10^{-15}$). (b) Transmission experiment at 72 Gbit/s per wavelength channel using QPSK. The EVM is plotted as a function of the transmitted distance. The insets show constellation diagrams of the best and worst performance. For both 16QAM and QPSK, error-free data transmission can be ensured if FEC with 7% overhead is considered.

modulation (16QAM) as modulation formats, and combine them with Nyquist pulse shaping [28,29]. At the receiver, digital signal processing is used for low-pass filtering, frequency offset compensation, clock recovery, polarization demultiplexing, dispersion compensation, and adaptive equalization. The quality of the received signal is evaluated by using the error-vector magnitude, which can be related to the bit error ratio [30].

The results of the data transmission experiments are summarized in Fig. 4. The 16QAM constellation diagrams for all wavelength channels and both polarizations are depicted along with the measured BER. Considering the symbol rate of 18 GBd on three wavelengths and two polarizations, we obtain an aggregate data rate of 432 Gbit/s. Using QPSK, we also demonstrate data transmission with up to 80 km of single-mode fiber without including additional amplification or any other means of signal regeneration. Figure 4(b) shows the EVM as a function of distance for a transmission at 216 Gbit/s. For distances of up to 80 km, the EVM remains below 19.2%, which corresponds to a BER below 10^{-7} [30]. In both cases, error-free data transmission can be ensured if forward error correction with 7% overhead is considered.

It is remarkable that data transmission on the side lines exhibits the same performance as on the center line, leading to data rates of 144 Gbit/s for each carrier—the highest value achieved for data transmission with Kerr combs so far. This unprecedented performance underlines the remarkable stability of the Turing patterns, which in this experiment did not require feedback stabilization. We may hence conclude that key performance parameters such as linewidth and relative intensity noise (RIN) are transferred from the pump to the newly generated modes. In this study, we have used only the first-order side modes (lines ±1), but higher-order spectral lines could be used as well. It is also important to note that optical Turing patterns are robust enough to enable transmission of data without further regeneration over 80 km.

In conclusion, we have demonstrated that optical Kerr frequency combs based on Turing patterns originating from a crystalline whispering-gallery-mode disk resonator are suitable sources for optical fiber data transmission, and allow for coherent data transmission using advanced modulation formats at up to 144 Gbit/s per wavelength channel. In particular, we anticipate that this comb generator could be of high interest for future optical fiber networks as it provides a path toward simple, compact, low-cost, energy-efficient, and reconfigurable multiwavelength sources for optical WDM data transmission systems within or between data centers [31].

C. K. and Y. K. C. acknowledge financial support from the European Research Council (ERC) through the projects EnTeraPIC and NextPhase/Versyt, respectively. C. K. acknowledges support from the Alfried Krupp von Bohlen und Halbach Foundation. J. P. and C. K. acknowledge support from the Center for Functional Nanostructure (CFN), from the Karlsruhe School of Optics and Photonics (KSOP), from the Helmholtz International Research School of Teratronics (HIRST), from the Karlsruhe Nano-Micro Facility (KNMF), from the EU-FP7 project Big Pipes, and from the initiative and networking fund of the Helmholtz Association. Y. K. C. acknowledges support from the Centre National d'Etudes Spatiales (CNES) through the project SHYRO, from the Région de Franche-Comté, and from the Labex ACTION funded by ANR.

J. P. and A. C. have provided equal contribution to this work.

*Present address: NIST, Boulder, CO 80305, USA.
†christian.koos@kit.edu
‡yanne.chembo@femto-st.fr

[1] P. Del'Haye, A. Schliesser, O. Arcizet, T. Wilken, R. Holzwarth, and T. J. Kippenberg, Optical frequency comb generation from a monolithic microresonator, Nature (London) **450**, 1214 (2007).
[2] Y. K. Chembo, D. V. Strekalov, and N. Yu, Spectrum and Dynamics of Optical Frequency Combs Generated with Monolithic Whispering Gallery Mode Resonators, Phys. Rev. Lett. **104**, 103902 (2010).
[3] Y. K. Chembo and N. Yu, Modal expansion approach to optical-frequency-comb generation with monolithic whispering-gallery-mode resonators, Phys. Rev. A **82**, 033801 (2010).
[4] T. Kippenberg, R. Holzwarth, and S. Diddams, Microresonator-based optical frequency comb, Science **332**, 555 (2011).
[5] F. Ferdous, H. Miao, D. E. Leaird, K. Srinivasan, J. Wang, L. Chen, L. T. Varghese, and A. M. Weiner, Spectral line-by-line pulse shaping of on-chip microresonator frequency combs, Nat. Photonics **5**, 770 (2011).
[6] A. A. Savchenkov, A. B. Matsko, W. Liang, V. S. Ilchenko, D. Seidel, and L. Maleki, Kerr combs with selectable central frequency, Nat. Photonics **5**, 293 (2011).
[7] J. Li, H. Lee, T. Chen, and K. J. Vahala, Low-Pump-Power, Low-Phase-Noise, and Microwave to Millimeter-Wave Repetition Rate Operation in Microcombs, Phys. Rev. Lett. **109**, 233901 (2012).
[8] T. Herr, K. Hartinger, J. Riemensberger, C. Y. Wang, E. Gavartin, R. Holzwarth, M. L. Gorodetsky, and T. J. Kippenberg, Universal formation dynamics and noise of Kerr-frequency combs in microresonators, Nat. Photonics **6**, 480 (2012).
[9] P. Del'Haye, S. B. Papp, and S. A. Diddams, Hybrid Electro-Optically Modulated Microcombs, Phys. Rev. Lett. **109**, 263901 (2012).
[10] D. J. Moss, R. Morandotti, A. L. Gaeta, and M. Lipson, New CMOS-compatible platforms based on silicon nitride and Hydex for nonlinear optics, Nat. Photonics **7**, 597 (2013).
[11] P.-H. Wang, F. Ferdous, H. Miao, J. Wang, D. E. Leaird, K. Srinivasan, L. Chen, V. Aksyuk, and A. M. Weiner, Observation of correlation between route to formation, coherence, noise, and communication performance of Kerr combs, Opt. Express **20**, 29284 (2012).
[12] J. Levy, K. Saha, Y. Okawachi, M. Foster, A. Gaeta, and M. Lipson, High-performance silicon-nitride-based multiple-wavelength source, IEEE Photonics Technol. Lett. **24**, 1375 (2012).
[13] J. Pfeifle *et al.*, Coherent terabit communications with microresonator Kerr frequency combs, Nat. Photonics **8**, 375 (2014).
[14] A. Coillet, I. Balakireva, R. Henriet, K. Saleh, L. Larger, J. M. Dudley, C. R. Menyuk, and Y. K. Chembo, Azimuthal Turing patterns, bright and dark cavity solitons in Kerr combs generated with whispering-gallery-mode resonators, IEEE Phot. J. **5**, 6100409 (2013).
[15] C. Godey, I. V. Balakireva, A. Coillet, and Y. K. Chembo, Stability analysis of the spatiotemporal Lugiato-Lefever model for Kerr optical frequency combs in the anomalous and normal dispersion regimes, Phys. Rev. A **89**, 063814 (2014).
[16] T. Herr, V. Brasch, J. D. Jost, C. Y. Wang, N. M. Kondratiev, M. L. Gorodetsky, and T. J. Kippenberg, Temporal solitons in optical microresonators, Nat. Photonics **8**, 145 (2014).
[17] A. M. Turing, The chemical basis of morphogenesis, Phil. Trans. R. Soc. B **237**, 37 (1952). The chemical patterns described by Turing in this seminal work on morphogenesis are mathematically identical to the optical patterns leading to primary combs (rolls). In optics, the process leading to these patterns is sometimes referred to as modulational instability.
[18] L. A. Lugiato and R. Lefever, Spatial Dissipative Structures in Passive Optical Systems, Phys. Rev. Lett. **58**, 2209 (1987).
[19] A. B. Matsko, A. A. Savchenkov, W. Liang, V. S. Ilchenko, D. Seidel, and L. Maleki, Mode-locked Kerr frequency combs, Opt. Lett. **36**, 2845 (2011).
[20] Y. K. Chembo and C. R. Menyuk, Spatiotemporal Lugiato-Lefever formalism for Kerr-comb generation in whispering-gallery-mode resonators, Phys. Rev. A **87**, 053852 (2013).
[21] S. Coen, H. G. Randle, T. Sylvestre, and M. Erkintalo, Modeling of octave-spanning Kerr frequency combs using a generalized mean-field Lugiato–Lefever model, Opt. Lett. **38**, 37 (2013).
[22] A. B. Matsko, A. A. Savchenkov, N. Yu, and L. Maleki, Whispering-gallery-mode resonators as frequency references. I. Fundamental limitations, J. Opt. Soc. Am. B **24**, 1324 (2007).
[23] A. A. Savchenkov, A. B. Matsko, V. S. Ilchenko, N. Yu, and L. Maleki, Whispering-gallery-mode resonators as frequency references. II. Stabilization, J. Opt. Soc. Am. B **24**, 2988 (2007).
[24] A. Coillet and Y. K. Chembo, Routes to spatiotemporal chaos in Kerr optical frequency combs, Chaos **24**, 013113 (2014).
[25] A. Coillet and Y. K. Chembo, On the robustness of phase locking in Kerr optical frequency combs, Opt. Lett. **39**, 1529 (2014).
[26] Note that our discrete first-order coherence function $\hat{g}_k^{(1)}$ has exactly the same physical meaning as the classical first-order coherence function $g^{(1)}(T)$. However, it is not its discrete counterpart in the strict sense. The reason is that $g^{(1)}(T)$ is theoretically defined for infinite and continuous time traces, while in our case, we define the coherence function $\hat{g}_k^{(1)}$ using a finite set of discretely distributed snapshots. This induces an artifactual loss of coherence for large k that has to be compensated through renormalization. See the Supplemental Material [27].
[27] See the Supplemental Material at http://link.aps.org/supplemental/10.1103/PhysRevLett.114.093902 for more mathematical details.
[28] R. Schmogrow *et al.*, Real-time software-defined multi-format transmitter generating 64QAM at 28 GBd, IEEE Photonics Technol. Lett. **22**, 1601 (2010).
[29] R. Schmogrow *et al.*, Real-time Nyquist pulse generation beyond 100 Gbit/s and its relation to OFDM, Opt. Express **20**, 317 (2012).
[30] R. Schmogrow *et al.*, Error vector magnitude as a performance measure for advanced modulation formats, IEEE Photonics Technol. Lett. **24**, 61 (2012); Corrections to "Error vector magnitude as a performance measure for advanced modulation formats" [Jan 1, 2012 61-63] , IEEE Photonics Technol. Lett. **24**, 2198(E) (2012).
[31] D. Hillerkuss *et al.*, Single-laser 32.5 Tbit/s nyquist WDM transmission, J. Opt. Commun. Netw. **4**, 715 (2012).